ROYAL SOCIETY OF CHEMISTRY

PAPER

Check for updates

Superhydrophobic granular filter media modified with mesoporous nanoparticles for magnetically guided oil cleanup†

Xin Zhang,‡[a] Huan Xiang,‡[a] Xing Huang,[a] Chuanbo Hu,*[ab] Zhongmei Xu,[a] Huawei Yin,[a] Tingzhen Li*[a] and Kangning Ren ⓘ *[bcd]

The frequent occurrence of marine oil spills and the discharge of oily industrial wastewater have resulted in severe environmental pollution and ecological crises. Conventional oil–water separation methods often struggle to balance high separation efficiency with material recyclability when dealing with large-scale oil contamination. Consequently, the development of efficient, recyclable, and economically viable oil–water separation materials has become an urgent challenge. In this study, a superhydrophobic/oleophilic composite ceramic particle filter medium (OFMSPsC) was synthesized using the chemical grafting method, incorporating mesoporous silica and magnetic Fe_3O_4 nanoparticles. The material surface was further modified with octadecyltrimethoxysilane (OTMS), significantly enhancing its hydrophobicity and stability. Characterization results revealed that OFMSPsC exhibits excellent superhydrophobic properties, with a contact angle of 156.6°, and favorable magnetic responsiveness, with a saturation magnetization of 1.173 emu g^{-1}. Additionally, the material demonstrated outstanding resistance to acidic and alkaline conditions, ultrasonic treatment, and mechanical abrasion. In oil–water separation experiments, OFMSPsC achieved over 93% separation efficiency and maintained stable performance after multiple reuse cycles. Furthermore, the embedded magnetic nanoparticles facilitated rapid recovery of the material using an external magnetic field, greatly enhancing its reusability and operational convenience. Overall, the fabricated OFMSPsC material shows great potential for applications in environmental remediation and industrial oil spill cleanup.

1. Introduction

In recent decades, marine oil spills and the discharge of oily industrial wastewater have become increasingly frequent, giving rise to severe environmental pollution and ecological crises.[1,2] Petroleum-based pollutants not only disrupt aquatic habitats and intensify eutrophication but can also bioaccumulate along the food chain, ultimately posing threats to human health.[3,4] Conventional oil–water separation methods, such as gravity settling, flotation, and membrane filtration, often struggle to maintain both high separation efficiency and satisfactory material recovery in the face of highly viscous, multi-component, or large-scale oil contamination.[5,6] Consequently, there is an urgent need for the development of advanced separation materials and technologies to fundamentally improve treatment efficacy and reduce secondary pollution.

Inspired by the special wettability observed on biological surfaces in nature, researchers have devised various super-wetting materials for separating oil–water mixtures.[7–9] For instance, lotus leaves and rose petals exhibit exceptional superhydrophobic/superoleophilic properties attributable to their hierarchical micro/nanostructures and low surface energy. In recent years, significant progress has been made in the research of superhydrophobic materials for oil–water separation, which has become a key technology for addressing marine oil spills and industrial oily wastewater pollution. Superhydrophobic materials, characterized by a water contact angle greater than 150°, leverage their unique surface properties to preferentially adsorb the oil phase in oil–water mixtures, thereby achieving highly efficient separation. These materials not only effectively handle high-viscosity, multicomponent, or large-scale oil contamination but also offer advantages such as reusability and environmental friendliness, making them

[a]Key Laboratory of Water Environment Evolution and Pollution Control in Three Gorges Reservoir, School of Environmental and Chemical Engineering, Chongqing Three Gorges University, Chongqing 404100, China. E-mail: huchuanbo@126.com; litingzhen@163.com

[b]Department of Chemistry, Hong Kong Baptist University, Kowloon Tong, Hong Kong 999077, China. E-mail: kangningren@hkbu.edu.hk

[c]State Key Laboratory of Environmental and Biological Analysis, Hong Kong Baptist University, Hong Kong 999077, China

[d]HKBU Institute of Research and Continuing Education, Shenzhen 518057, China

† Electronic supplementary information (ESI) available. See DOI: https://doi.org/10.1039/d5ta02783g

‡ Xin Zhang and Huan Xiang made equal contributions to this work and are both recognized as first authors.

highly promising for applications in environmental protection and industrial wastewater treatment. The importance of superhydrophobic materials in oil–water separation applications is undeniable. They significantly enhance separation efficiency, reduce secondary pollution, and lower treatment costs. With the continuous advancement of nanotechnology and materials science, researchers have developed various types of superhydrophobic materials, including zero-dimensional nanoparticles,[10] one-dimensional fibrous structures,[11] two-dimensional separation membranes,[12] and three-dimensional absorbent media.[13] Through self-assembly, Yuan *et al.*[14] created a free-standing nanowire membrane that exhibits a superhydrophobic water contact angle of 172° and can selectively absorb oil up to 20 times its own weight, while also demonstrating excellent recyclability. Zhang *et al.*[15] synthesized a quartz sand with superhydrophobic and superoleophilic properties through a two-step modification process, resulting in a water contact angle of 165° and an oil–water separation efficiency greater than 85% after several cycles. Using a simple two-step immersion method, Xiao *et al.*[16] produced a melamine sponge characterized by superhydrophobic and superlipophilic properties. The modified sponge presented a static water contact angle of 156° and enabled rapid, efficient separation of chloroform and water, with nearly complete removal of the chloroform phase within seconds. Moreover, it maintained robust hydrophobicity under acidic, alkaline, and organic solvent conditions. Despite the remarkable achievements of superhydrophobic materials in oil–water separation, several challenges and limitations remain. One major concern is the insufficient stability, reusability, and recyclability of many superhydrophobic materials, particularly when dealing with complex or large-scale oil contamination scenarios. Furthermore, the high fabrication costs of these materials hinder their widespread practical application. Additionally, the long-term performance of certain superhydrophobic materials remains inadequate under harsh environmental conditions, such as exposure to strong acidic or alkaline media and elevated temperatures, necessitating further optimization. To address these limitations, the integration of magnetic nanoparticles into superhydrophobic/superoleophilic materials has emerged as a research hotspot, as the external magnetic field can be leveraged to enable rapid recovery and regeneration following separation operations, thereby mitigating secondary pollution and reducing overall costs.[17,18] Combining bioinspired design and functional modification strategies further refines the surface architecture and wetting behavior of filter media, particularly opening up new opportunities for the advancement of effective and reusable granular particle-based substrates.

Among the available substrate materials, dispersed ceramic particles have attracted attention owing to their remarkable chemical stability and mechanical strength.[19] Compared with membranes or fibrous supports, these particle-based systems exhibit improved flexibility for large-scale deployment in complex aqueous environments; furthermore, their porous framework provides ample surface area and robust anchoring sites for subsequent functional coatings.[20] Meanwhile, mesoporous materials demonstrate notably high surface area, tunable pore channels, and excellent chemical stability, making them highly advantageous for applications in oil–water separation—particularly under superhydrophobic conditions.[21] These materials offer plentiful adsorption and storage sites for the oil phase and can be further functionalized to tailor their wettability.[22] Nonetheless, challenges remain in recovering and reusing mesoporous particles after separation if they rely solely on inherent superhydrophobic or superoleophilic features. Embedding magnetic nanoparticles (*e.g.*, Fe_3O_4) within such mesoporous frameworks enables the use of external magnetic fields for swift collection, substantially reducing the risk of secondary contamination.

On this basis, the present study systematically prepared magnetic mesoporous silica submicron particles (FMSPs) and effectively combined them with porous ceramic particles *via* an OTMS-mediated grafting strategy to construct a novel, dispersed oil–water separation material endowed with superhydrophobic/superoleophilic properties and magnetic recyclability. Optimization efforts focused on determining the ideal ratio of Fe_3O_4 nanoparticles to the mesoporous silica scaffold, improving FMSP loading efficiency onto the ceramic substrate, and adjusting OTMS concentrations. Comprehensive characterization, including chemical composition, microscopic morphology, and surface roughness, was conducted to assess the resulting composite. Experimental outcomes demonstrate that, under an external magnetic field, the material achieves rapid, high-efficiency oil–water separation while maintaining excellent recyclability and structural integrity, thus offering a promising approach for large-scale and frequent oil pollution remediation.

2. Materials and methods

2.1. Materials

Iron(III) oxide (Fe_3O_4) nanoparticles with sizes of 20 nm and 50 nm, octadecyltrimethoxysilane (OTMS) were delivered by Shanghai Macklin Biochemical Technology Co., Ltd. Cetyltrimethylammonium bromide (CTAB), chloroform, toluene and *n*-hexane were obtained from Chongqing Chuandong Chemical Co., Ltd, while tetraethyl orthosilicate (TEOS) was provided by Yousuo Chemical Technology Co., Ltd (Shandong). Porous ceramic particles with a size range of 0.5–1 mm were obtained from local manufacturers. Analytical grade aqueous ammonia solution ($NH_3 \cdot H_2O$), ethanol (C_2H_6O) and HCl were bought from Chengdu Chron Chemical Co., Ltd. Cyclohexane was bought from Xilong Scientific Co., Ltd, and petroleum ether was procured from Guangzhou Jinyuan Chemical Co., Ltd. Edible oil was sourced from local suppliers. All chemicals were utilized in their received form without any additional purification.

2.2. Fabrication of magnetic mesoporous silica submicron particles

Using CTAB as template, TEOS as precursor, and $NH_3 \cdot H_2O$ as catalyst, magnetic mesoporous silica submicron particles were fabricated *via* the sol–gel strategy. Initially, 0.8 g of 20 nm Fe_3O_4 particles and 3.2 g of 50 nm Fe_3O_4 particles were dispersed in

This journal is © The Royal Society of Chemistry 2025

J. Mater. Chem. A, 2025, **13**, 23046–23058 | **23047**

a solution comprising 90 mL of ethanol and 150 mL of deionized water. The resulting mixture was subjected to ultrasonic treatment for 10 min to achieve a uniform dispersion. Afterwards, 4 g of CTAB and 25 mL of TEOS were incorporated and mixed thoroughly. Immediately afterwards, 25 mL of $NH_3 \cdot H_2O$ was added dropwise to catalyze the hydrolysis process. Following 3 h of stirring at 25 °C, the resultant product was subjected to filtration. The collected material was then dried at 105 °C and subsequently milled into a fine powder. The powder was calcined in a muffle furnace at 200 °C for 6 h, followed by a second stage at 600 °C for another 6 h. The final product was ground again to obtain Fe_3O_4/mesoporous SiO_2 particles (FMSPs). Additionally, for comparison, pure mesoporous silica particles (MSPs) without the incorporation of Fe_3O_4 were also prepared.

2.3. Preparation of superhydrophobic ceramic particles

The porous ceramic particles used as the filter media were pretreated to remove surface impurities. Ceramic particles were first ultrasonically cleaned in ethanol for 5 min, followed by another ultrasonic cleaning in distilled water for 5 minutes. The cleaned particles were then dried in an oven at 100 °C for 2 h. To further remove surface oxides, the dried particles were immersed in 1 mol per L hydrochloric acid solution (ceramic to hydrochloric acid mass ratio of 1 : 2) for 30 min. Following acid treatment, the particles were thoroughly rinsed with deionized water until the pH of the wash water reached 7. Finally, the particles were dried again at 100 °C for 2 h to obtain clean, pretreated porous ceramic particles.

A total of 0.5 g of FMSPs particles was dispersed in 25 mL of anhydrous ethanol and stirred at 35 °C for 30 min, followed by ultrasonic treatment for another 30 min. Subsequently, 0.74 mL of OTMS was added, and the suspension was stirred for 2 h. Following this, 5 g of porous ceramic particles was added to the mixture, which was then stirred for another 2 hours. The resulting mixture was placed in an oil bath maintained at 110 °C to ensure uniform heating and stirred until the ethanol was completely evaporated. The product was subsequently dried at 100 °C, and unbonded powder was removed using a 0.3 mm stainless steel sieve. Ultimately, the superhydrophobic/superoleophilic functional porous OTMS-modified FMSPs composite ceramic material (OFMSPsC) were successfully obtained. The fabrication process and synthetic route are illustrated in Fig. 1. Fig. 1b demonstrates that both the ceramic particles and FMSPs particles expose hydroxyl (–OH) groups on their surfaces. The hydrolyzed OTMS undergoes condensation reactions with these –OH groups on both components, forming stable Si–O–Si/ceramic bonds. This chemically immobilizes the FMSPs particles onto the ceramic substrate, permanently anchoring them while exposing hydrophobic alkyl chains. The ceramic composite prepared without OTMS modification was designated as FMSPsC-3. The optimal ratio of Fe_3O_4 nanoparticles, the optimal loading amount of FMSPs, and the optimal OTMS concentration were systematically investigated and optimized. The samples obtained were designated as OFMSPsC-1, OFMSPsC-2, and OFMSPsC-3, respectively.

2.4. Characterization

Transmission electron microscopy (TEM) images were captured using a JEOL JEM 2100F instrument. Scanning electron microscopy (SEM) imaging and Energy Dispersive X-ray Spectroscopy (EDX) were conducted with a ZEISS GeminiSEM 300 system. X-ray powder diffraction (XRD) patterns were collected using a Bruker D8 advance X-ray diffractometer. To evaluate wettability, contact angles were measured at ambient temperature with 2.5 μL liquid droplets on an SDC-350 instrument, and the results were averaged across five distinct sample regions. The surface topography of the samples was analyzed using confocal laser scanning microscopy (CLSM) on a KEYENCE VK-X150 platform. The chemical composition of the particles was characterized through X-ray photoelectron spectroscopy (XPS) on a Thermo Scientific K-Alpha spectrometer, in conjunction with thermal gravimetric analysis (TGA) performed using an STA 449F3 apparatus.

2.5. Oil–water separation test

The oil–water separation experiment, driven by gravity, utilized a filtration system consisting of a vacuum filtration flask and a glass funnel, as illustrated in Fig. 6a. The experimental mixture comprised 50 mL of organic liquids (such as n-hexane, cyclohexane, petroleum ether, toluene, and edible oil) colored with Sudan III, along with 50 mL of water stained with methylene blue. OFMSPsC-3 served as the filtering medium and was positioned inside a funnel. The oi–water mixture was then gradually introduced into the separation apparatus, with the separation process driven entirely by gravity. The magnetic recovery process consisted of: (1) ultrasonic cleaning in ethanol (5 min) to dissolve residual oil, (2) magnetic separation for material recovery (0.8 T), and (3) vacuum drying at 60 °C (2 h) to restore the material's porous structure. This procedure effectively maintained the separation performance while ensuring high recovery efficiency. The separation efficiency was determined by collecting the permeated oil and measuring its volume using the following formulas:[22,23]

$$Flux = \frac{V}{S \times t} \tag{1}$$

$$\eta = \frac{V_1}{V_0} \times 100\% \tag{2}$$

in this context, V represents the volume of the organic liquid (m^3), S indicates the effective contact area between the organic liquid and OFMSPs-3 (m^2), t denotes the filtration duration of the organic liquid (h), while V_1 and V_0 correspond to the mass of water in the mixture after and before filtration, respectively. The experiments were performed three times, and the average values are reported.

The adsorption capacity of OFMSPsC-3 for typical oils was also experimentally measured. A dried OFMSPsC-3 sample (mass = m_0) was immersed in various oil types (e.g., n-hexane, cyclohexane, edible oil) for 5 minutes. After draining excess oil, the sample was reweighed (m_1), and the oil adsorption capacity (Q) was calculated using the formula:
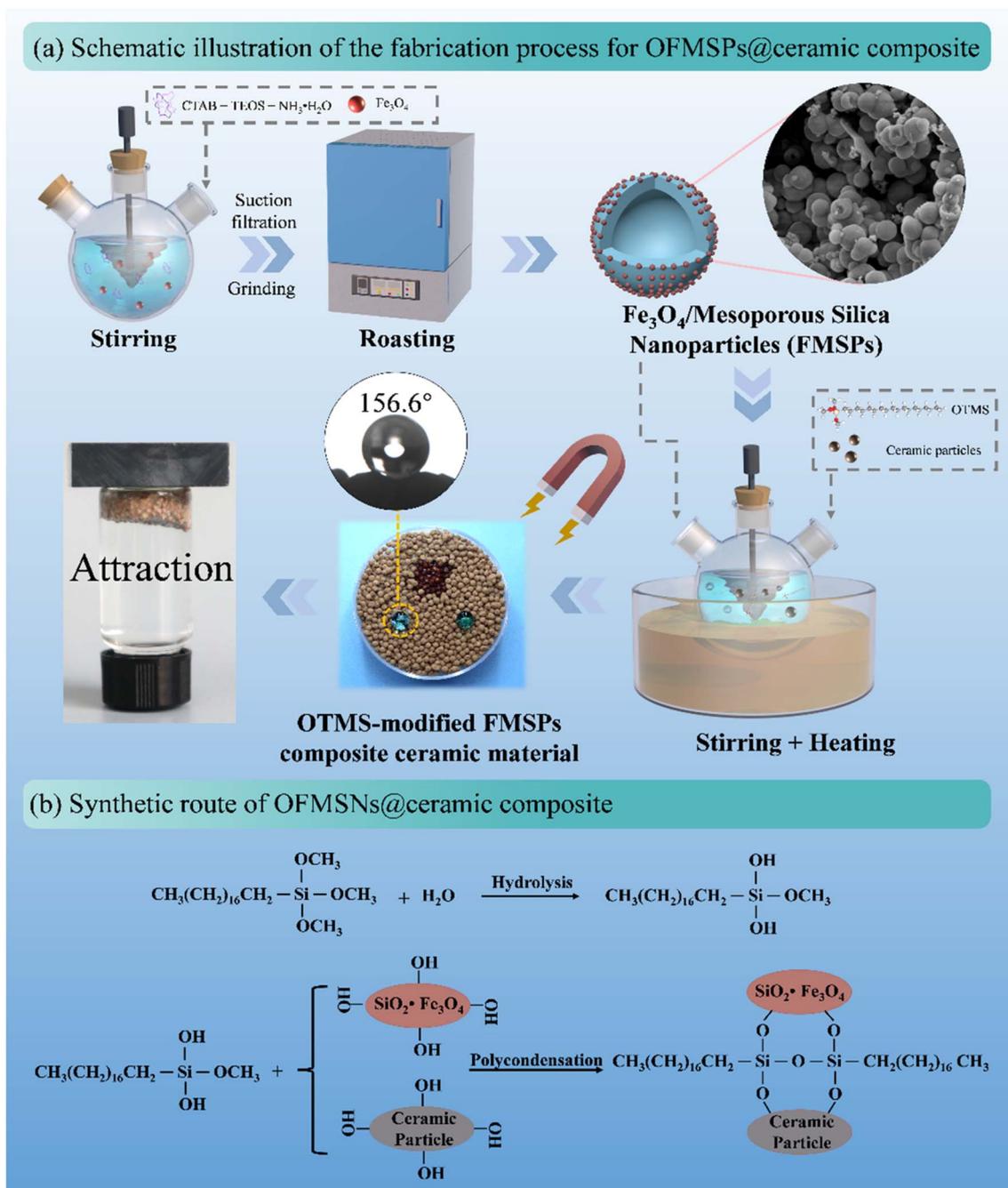
23048 | *J. Mater. Chem. A*, 2025, **13**, 23046–23058

This journal is © The Royal Society of Chemistry 2025

Fig. 1 (a) Schematic illustration of the fabrication process and (b) synthetic route for OFMSPsC.

$$Q = \frac{(m_1 - m_0)}{m} \qquad (3)$$

3. Results and discussion

3.1. Chemical features and morphologies

To validate the chemical bonds and compositional modifications achieved during the synthesis process, XRD, FTIR, EDS, and XPS characterization techniques were employed, as shown

in Fig. 2. Fig. 2a exhibits the XRD patterns of FMSPs and MSPs. Both MSPs and FMSPs exhibit a broad peak at around $2\theta \sim 23°$, corresponding to the amorphous silica structure.[24] In the case of FMSPs, the peaks at $2\theta = 30.6°$, $36.1°$, $43.9°$, $54.3°$, $57.7°$, and $63.5°$ are attributed to the (220), (311), (400), (422), (511), and (440) crystal planes of Fe_3O_4, respectively, indicating that Fe_3O_4 is loaded on the mesoporous silica.[25] As shown in Fig. 2b, MSPs exhibit characteristic absorption peaks of silica, including the –OH stretching vibration observed at 3431 cm^{-1}, along with the asymmetric and symmetric Si–O–Si stretching vibrations at 1077 cm^{-1} and 791 cm^{-1}, respectively.[26–28] Upon incorporation

This journal is © The Royal Society of Chemistry 2025

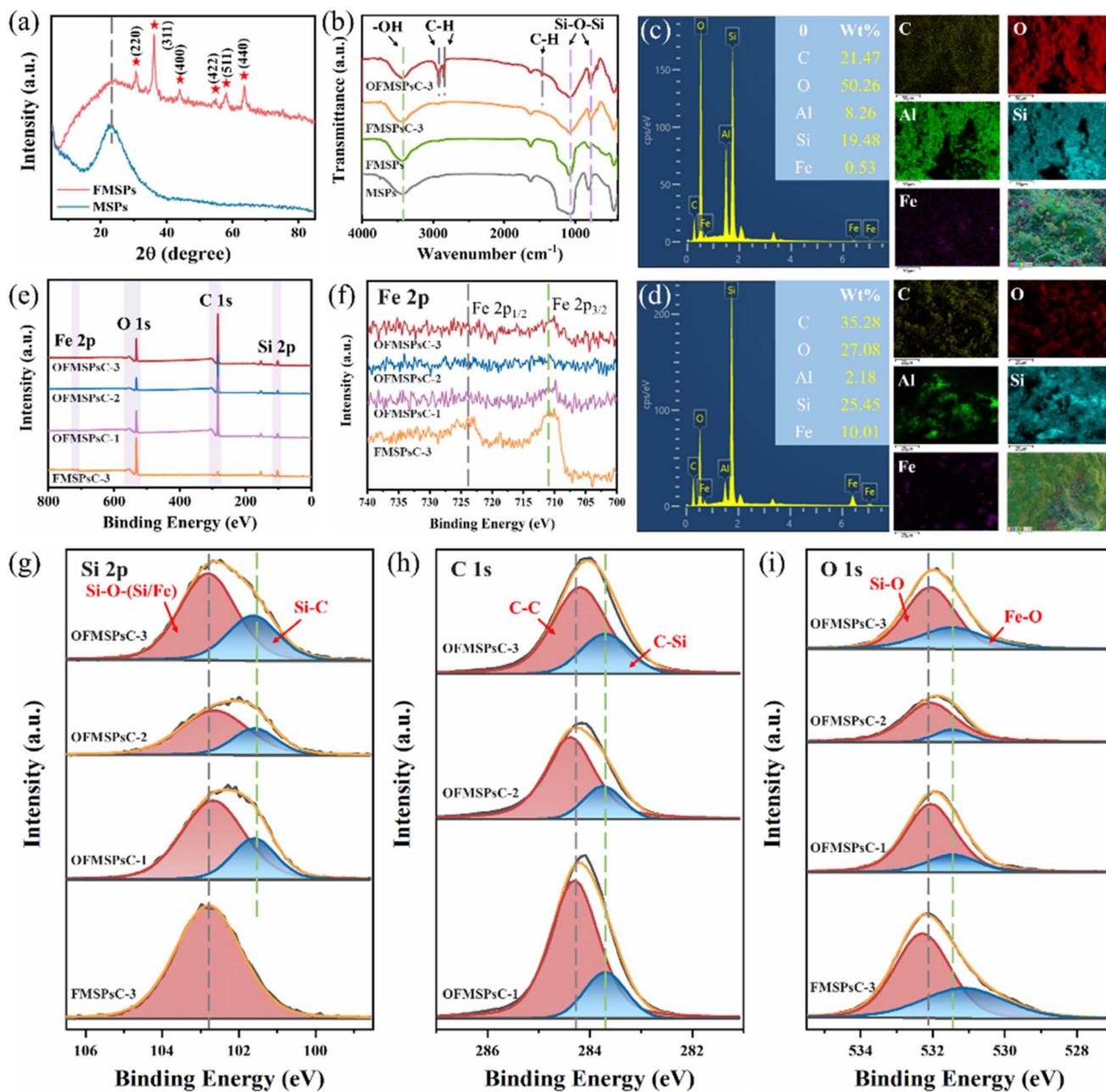*J. Mater. Chem. A*, 2025, **13**, 23046–23058 | **23049**

Fig. 2 (a) XRD patterns of MSPs and FMSPs. (b) FTIR spectra of MSPs, FMSPs, FMSPsC and OFMSPsC. EDS spectra and mapping of (c) FMSPsC and (d) OFMSPsC. (e) XPS spectra of FMSPsC-3, OFMSPsC-1, OFMSPsC-2, and OFMSPsC-3. The high-resolution XPS spectra of (f) Fe 2p, (g) Si 2p, (h) C 1s, and (i) O 1s.

of Fe_3O_4, no new absorption peaks were detected, likely due to overlap with the silica framework signals, as suggested by XRD, EDS, and XPS analyses. In the case of the OTMS-modified OFMSPsC-3, the appearance of new absorption peaks at 2920 cm^{-1}, 2849 cm^{-1}, and 1463 cm^{-1}, which are attributed to the asymmetric, symmetric, and bending C–H stretching vibrations of OTMS alkyl groups, serves as direct evidence of successful OTMS grafting.[29,30] As depicted in Fig. 2c and d, the elemental composition of FMSPsC-3 and OFMSPsC-3 was investigated using EDS analysis. By comparison, the increase in C content in OFMSPsC-3 (35.28 wt%) provides further evidence

of the successful grafting of OTMS onto the surface. Furthermore, the increases in Fe (10.01 wt%) and Si contents (25.45 wt%), along with the decrease in Al content (2.18 wt%), demonstrate that OTMS served as a chemical bridge. This bridging facilitated the enhanced binding of FMSPs submicron particles to the ceramic substrate, leading to more uniform coverage and multiscale integration.

Fig. 2e presents the XPS spectra of FMSPsC-3 and OTMS-modified OFMSPsC-1, OFMSPsC-2, and OFMSPsC-3. In the spectrum of FMSPsC-3, the elements Si (Si2p, 102.8 eV), C (C 1s, 284.3 eV), O (O 1s, 532.1 eV), and Fe (Fe 2p, 710.4 eV) were

observed. After OTMS modification, the C 1s peak intensity of OFMSPsC-1, OFMSPsC-2, and OFMSPsC-3 showed a significant increase, demonstrating that the modification led to a rise in carbon content, which is consistent with the chemical structure of OTMS. Fig. 2f presents the high-resolution XPS spectrum of Fe 2p, revealing two distinct signals at 710.6 eV and 725.4 eV, which are associated with the characteristic double peaks of Fe $2p_{3/2}$ and Fe $2p_{1/2}$ in Fe_3O_4.[31,32] In the Si 2p spectra (Fig. 2g), FMSPsC-3 exhibits a single peak at 102.8 eV, which corresponds to Si–O–(Si/Fe) bonds.[33,34] This peak is attributed to the silica framework, interactions between silica and Fe_3O_4 nanoparticles, and interactions between FMSPs and the ceramic substrate. In contrast, a new peak emerges at 101.6 eV in the OFMSPsC-1, OFMSPsC-2, and OFMSPsC-3 spectra, which corresponds to the Si–C groups of OTMS.[35] In the high-resolution C 1s spectra of OFMSPsC-1, OFMSPsC-2, and OFMSPsC-3 (Fig. 2h), peaks at 283.7 eV and 284.2 eV are observed, which correspond to C–Si and C–C groups, respectively.[36] These results further confirm that OTMS was successfully grafted onto the surface, introducing abundant hydrophobic groups that contribute to the superhydrophobic properties of the ceramic particles. Additionally, as shown in Fig. 2i, the O 1s spectra were resolved into two peaks at 532.1 eV and 531.5 eV, corresponding to Si–O in the silica framework and Fe–O in Fe_3O_4, respectively.[37,38] Collectively, these results demonstrate that OTMS modification not only introduced hydrophobic functional groups but also enhanced the chemical bonding and interactions between FMSPs and the ceramic substrate, ensuring improved structural stability and functional integration.

To investigate the surface morphology of FMSPs and structural evolution during different modification stages, SEM, TEM, and CLSM analyses were conducted. Fig. 3a–f show the SEM images of MSPs, FMSPs, FMSPsC-3, OFMSPsC-1, OFMSPsC-2, and OFMSPsC-3. As shown in Fig. 3a, MSPs exhibit a smooth and uniform spherical morphology. The TEM image (Fig. 3g) further reveals their hollow spherical mesoporous submicron structure. Particle size distribution analysis (Fig. 3i) reveals that the unmodified MSPs exhibit a narrow size distribution with an average diameter of 0.65 $\pm$ 0.21 μm, confirming their high uniformity. This homogeneity is critical for ensuring consistent mesoporous structure and surface functionality. After loading Fe_3O_4 nanoparticles (Fig. 3b), the nanoparticles are anchored onto the MSPs surfaces, reducing the average particle diameter to 0.53 $\pm$ 0.15 μm (Fig. 3j). The tighter distribution further validates the stability of the functionalization process. TEM characterization (Fig. 3h) confirms that Fe_3O_4 nanoparticles are uniformly distributed on the MSPs surfaces while preserving the silica hollow structure. During the grafting process onto the ceramic substrate, Fig. 3c shows that FMSPsC-3 exhibits inadequate coverage and surface uniformity, primarily because the bonding between FMSPs particles and both the substrate and each other relies mainly on physical adsorption or a limited number of functional groups. In contrast, as shown in Fig. 3d–f, OFMSPsC-1, OFMSPsC-2, and OFMSPsC-3 employ OTMS to form a stable functional network between the FMSPs and the ceramic substrate, resulting in not only a more uniform distribution and tighter bonding of FMSPs but also, through the optimized conditions, a progressively denser stacking and connection of FMSPs on the substrate, thereby enhancing
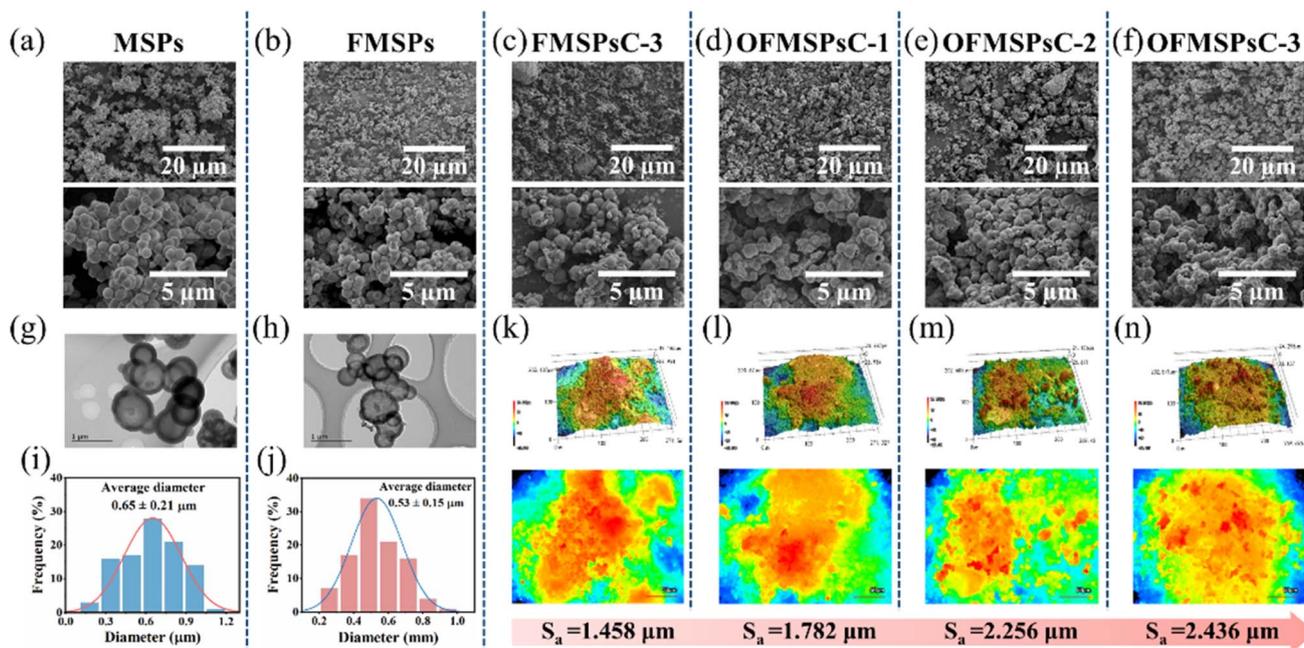

Fig. 3 (a–f) SEM images of MSPs, FMSPs, FMSPsC-3, OFMSPsC-1, OFMSPsC-2, and OFMSPsC-3. (g and h) TEM images of MSPs and FMSPs. (i and j) Particle size distributions of MSPs and FMSPs. (k–n) 3D CLSM surface topography and corresponding average roughness (S_a) values of FMSPsC-3, OFMSPsC-1, OFMSPsC-2, and OFMSPsC-3.

This journal is © The Royal Society of Chemistry 2025

J. Mater. Chem. A, 2025, **13**, 23046–23058 | **23051**

surface coverage. As presented in Fig. 3k–n, the CLSM images of FMSPsC-3, OFMSPsC-1, OFMSPsC-2, and OFMSPsC-3 indicate that the average surface roughness (S_a) increases markedly with the progressive optimization of OTMS bridging and processing conditions. Specifically, S_a rises from 1.458 μm for FMSPsC-3 to 1.782 μm, 2.256 μm, and 2.436 μm for OFMSPsC-1, OFMSPsC-2, and OFMSPsC-3, respectively, corroborating the SEM observations of increasingly denser surface particle accumulation. Overall, OTMS acts as a "molecular bridge" between the particles and the ceramic substrate, effectively improving both surface coverage and structural stability of the resultant material.

3.2. Wettability and durability

Fig. 4a compares the wettability performance of FMSPsC-3, OFMSPsC-1, OFMSPsC-2, and OFMSPsC-3. FMSPsC-3 displays a water contact angle (WCA) of 0, signifying its hydrophilic nature, which is due to the high concentration of hydroxyl groups present on the surface. Following the modification with OTMS, the WCA of OFMSPsC-1 increases significantly to 147.5 ± 3.0°, with a sliding angle (SA) of 7.8 ± 1.6°. Further optimization of the FMSPs loading results in an increase in WCA to 153.7 ± 1.6° and a decrease in SA to 4.9 ± 1.3° for OFMSPsC-2. Subsequently, by optimizing the OTMS amount, OFMSPsC-3 achieves the highest WCA of 156.6 ± 1.8° and a reduced SA of 3.7 ± 1.6°, demonstrating superior superhydrophobic

performance. The degree of OTMS functionalization and the FMSPs loading directly influence the formation of surface roughness and the concentration of low surface energy groups. Specifically, the optimized OTMS amount on OFMSPsC-3 leads to more effective surface coverage and stronger chemical bonding, resulting in a hierarchical micro/nanostructure that enhances its superhydrophobicity.

As shown in Fig. 4b, the silver mirror reaction was conducted to evaluate the superhydrophobic properties and air-cushion stability of OFMSPsC-1, OFMSPsC-2, and OFMSPsC-3, with FMSPsC-3 included as a control. Upon immersion in deionized water, FMSPsC-3 was completely wetted upon contact with water and dispersed into the liquid. In contrast, OFMSPsC-1, OFMSPsC-2, and OFMSPsC-3 exhibited significantly different behaviors. These dispersed samples aggregated into compact clusters upon immersion, showing a prominent "silver mirror" effect caused by total internal reflection from the trapped air layer.[39] OFMSPsC-3 displayed the most exceptional performance among the samples, forming a thicker, more uniform, and stable air-cushion layer. This can be attributed to the denser and more uniform grafting of hydrophobic alkyl chains introduced via OTMS modification, which created a robust barrier against water infiltration. Additionally, the higher hierarchical surface roughness of OFMSPsC-3 further enhanced the stability of the trapped air layer. These synergistic features allowed OFMSPsC-3 to maintain a stable Cassie–Baxter state, ensuring
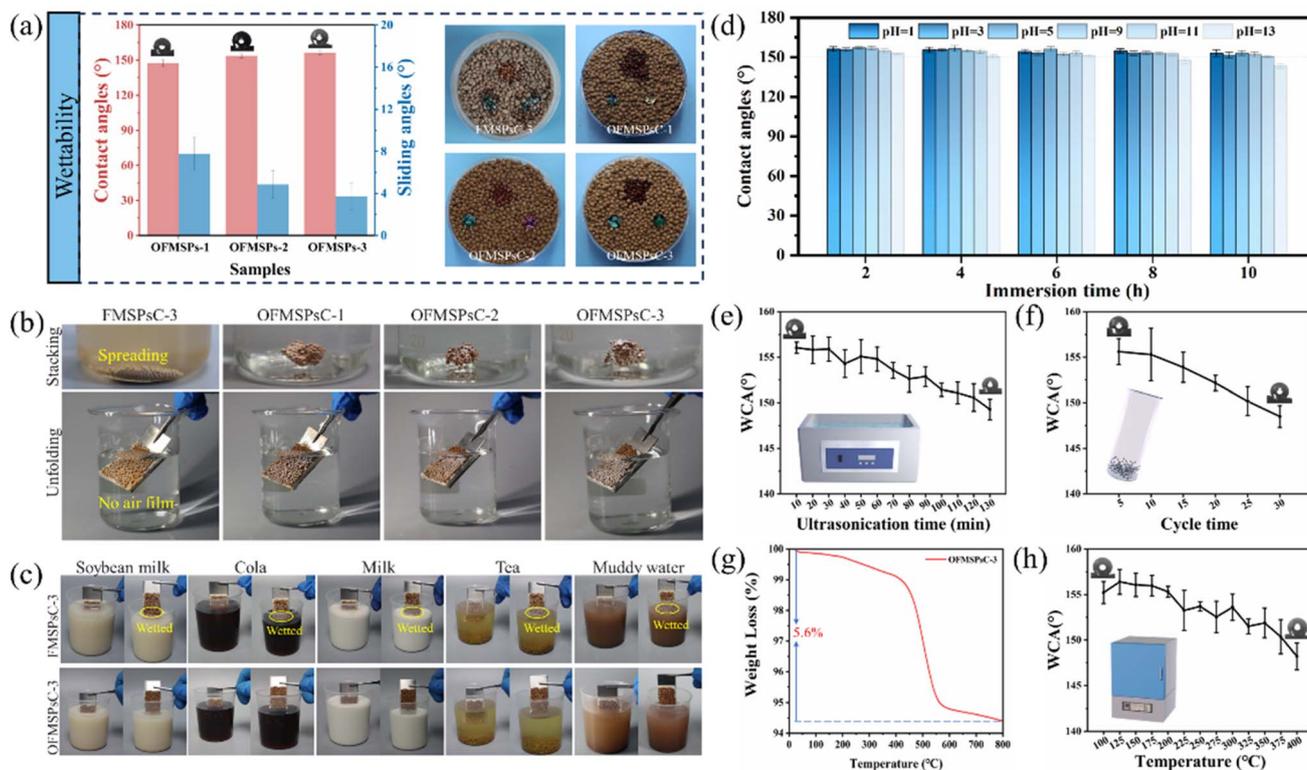

Fig. 4 (a) Water and oil droplet wetting behaviors on the surface of the FMSPsC-3, OFMSPsC-1, OFMSPsC-2 and OFMSPsC-3 and their WCA and WSA results. (b) Photographs of FMSPsC-3, OFMSPsC-1, OFMSPsC-2 and OFMSPsC-3 in water. (c) Direct antifouling tests on FMSPsC-3 and OFMSPsC-3. (d) Acid–alkali resistance tests. Mechanical stability evaluation via (e) ultrasonic tests and (f) collision tests. (g) TGA curve and (h) high-temperature resistance assessment of the OFMSPsC-3.

23052 | J. Mater. Chem. A, 2025, 13, 23046–23058

This journal is © The Royal Society of Chemistry 2025

superior water repellence and reliable anti-wetting performance.

The durability of the composite materials was comprehensively evaluated through a series of tests, including stain resistance, ultrasonic durability, acid–base immersion, and mechanical abrasion. These tests aimed to investigate the wettability retention of the samples under challenging conditions. To evaluate the anti-fouling performance of the materials, stain resistance tests were conducted using soybean milk, cola, milk, tea, and muddy water. As shown in Fig. 4c, FMSPsC-3 and OFMSPsC-3 were immersed in these liquids for 10 minutes to observe their resistance to contamination. FMSPsC-3 exhibited clear signs of being wetted in all the tested liquids, with water droplets spreading across its surface. Upon removal from the liquids, the surface of FMSPsC-3 remained wet, with residual liquid clinging to it, indicating poor resistance to fouling and wetting. In contrast, OFMSPsC-3 displayed remarkable anti-fouling properties. During immersion, the sample maintained a stable air-cushion layer on its surface, which was evident from the reflective "silver mirror" effect, indicating that the liquid did not penetrate its surface. Upon removal from the liquids, the surface of OFMSPsC-3 remained dry and free of residues, demonstrating excellent self-cleaning capabilities.

The acid–base resistance of OFMSPsC-3 was evaluated by submerging the samples in solutions of different pH levels (pH $= 1, 3, 5, 9, 11,$ and 13) for various time periods (2, 4, 6, 8, and 10 h). Post-immersion, the WCA was measured to evaluate the retention of superhydrophobicity under harsh chemical conditions. As depicted in Fig. 4d, OFMSPsC-3 maintained excellent superhydrophobicity across all pH levels, with WCA values consistently exceeding $143°$ even after 10 hours of immersion. Specifically, in highly alkaline conditions (pH $= 13$), the WCA slightly decreased to $151.2°$ after 6 hours, while in highly acidic environments (pH $= 1$), the WCA remained above $153.1°$ throughout the immersion period. In weak acidic and weak alkaline conditions, the CA values consistently stayed above $150°$, indicating optimal stability of OFMSPsC-3 in these environments. The outstanding acid–base resistance of OFMSPsC-3 can be attributed to the densely grafted alkyl chains, which form a hydrophobic barrier that effectively isolates corrosive liquids, thereby protecting the material from chemical degradation. This makes OFMSPsC-3 a promising candidate for applications exposed to acidic or alkaline solutions, such as industrial wastewater treatment or oil–water separation in chemically corrosive environments.

The ultrasonic durability of OFMSPsC-1, OFMSPsC-2, and OFMSPsC-3 was evaluated by subjecting the samples to ultrasonic treatment in deionized water (40 kHz, 150 W). Water contact angles (WCA) were measured every 10 min to monitor changes in superhydrophobicity over time. As shown in Fig. 4e, all samples exhibited a gradual decline in WCA with increasing ultrasonic exposure time. OFMSPsC-1 experienced the fastest decrease, with the WCA dropping below $140°$ after 50 min. OFMSPsC-2 maintained superhydrophobicity (WCA above $150°$) for up to 90 min. Notably, OFMSPsC-3 demonstrated the highest durability among the tested samples, retaining its superhydrophobicity for up to 120 min of ultrasonic exposure. This

superior ultrasonic durability of OFMSPsC-3 is attributed to the sufficient molecular entanglement between the hydrophobic grafted chains of OTMS and the FMSPs and ceramic substrate, which enhances the overall structural integrity of the surface, thereby ensuring prolonged maintenance of superhydrophobic properties under dynamic conditions. In addition, the impact resistance of the composite materials was evaluated by subjecting 50 g OFMSPsC-3 to mechanical stress within a cylindrical container (height 20 cm, diameter 4 cm). The container was shaken to simulate the mechanical forces and collisions that the materials might encounter in practical applications. The number of shakes was recorded, and the WCA was measured every 15 shakes as one cycle to evaluate the retention of superhydrophobic performance. After 375 shakes, the WCA of OFMSPsC-3 slightly decreased to $150.2°$ (as illustrated in Fig. 4f), demonstrating excellent mechanical stability. The remarkable mechanical stability of OFMSPsC-3 is due to the synergistic effects of chemical bonding and the surface structure. The extensive OTMS grafting not only reduced surface energy but also acted as a chemical bridge between FMSPs and the ceramic substrate, forming stronger covalent bonds that prevent detachment under mechanical stress. This ensures the long-term stability and durability of the material in mechanically demanding environments.

The thermal stability of OFMSPsC-3 was thoroughly examined using thermogravimetric analysis (TGA) and muffle furnace heating tests. TGA was performed in an air atmosphere over a temperature range of 22–800 °C to investigate the thermal decomposition behavior of OFMSPsC-3. As shown in Fig. 4g, the TGA curve exhibited two distinct weight loss stages, corresponding to the decomposition of different components within the composite. The first minor weight loss of approximately 0.3% occurred under 200 °C, attributed to the evaporation of physically adsorbed water and residual ethanol within the mesoporous structure.[40] The second, more significant weight loss of 5.3% commenced around 200 °C and continued up to 600 °C, corresponding to the thermal decomposition of organic functional groups, primarily from OTMS.[41] This indicates that the submicron silica spheres, Fe_3O_4 nanoparticles, and ceramic substrate possess high thermal stability. Additionally, thermal stability was further assessed by subjecting OFMSPsC-3 to heating cycles in a muffle furnace, gradually increasing the temperature from 25 to 450 °C and maintaining it for 30 min per cycle. Following each heating cycle, the samples were allowed to cool to room temperature, after which the WCA was measured to assess wettability. As presented in Fig. 4h, OFMSPsC-3 maintained an excellent superhydrophobicity with WCA values above $155°$ even when heated up to 200 °C. However, when the temperature exceeded 200 °C, a significant reduction in WCA was observed, dropping to approximately $148.5°$ at 400 °C, which led to a loss of superhydrophobicity. This transition reflects the thermal decomposition of the OTMS alkyl chains, which compromises the hierarchical roughness and surface energy necessary to maintain the Cassie–Baxter state. Nevertheless, OFMSPsC-3 demonstrated remarkable thermal stability, retaining its structural integrity and

This journal is © The Royal Society of Chemistry 2025

J. Mater. Chem. A, 2025, 13, 23046–23058 | 23053

superhydrophobic characteristics up to 200 °C, making it suitable for applications requiring resistance to high temperatures.

3.3. Magnetic oil absorption and recovery

The magnetic recovery capability of OFMSPsC primarily originates from the embedded magnetic Fe_3O_4 nanoparticles. These nanoparticles confer exceptional magnetic responsiveness to the material, enabling rapid attraction and recovery under an external magnetic field. This feature is particularly crucial for oil–water separation processes, as it not only facilitates swift material recovery and significantly enhances operational efficiency, but also avoids potential secondary contamination associated with traditional recovery methods while reducing overall operational costs. As shown in Fig. 5a and b, the magnetization curves of pure ceramic particles, FMSPsC-3, and OFMSPsC-3 are presented respectively. Pure ceramic particles exhibit negligible magnetization, whereas OFMSPsC-3 achieves a saturation magnetization of approximately 1.173 emu g^{-1}, demonstrating sufficient magnetic responsiveness to enable effective magnetic recovery. This significant magnetization is attributable to the successful incorporation of magnetic Fe_3O_4 nanoparticles within the OFMSPsC-3 matrix. On the other hand, FMSPsC-3 displayed a considerably lower magnetization compared to OFMSPsC-3. This reduction in magnetic response is due to the insufficient grafting of FMSPs onto the ceramic substrate, which impairs the uniform distribution and effectiveness of the magnetic nanoparticles, thereby diminishing its overall magnetic properties. Fig. 5c, d and Video S1† illustrate the real-time oil absorption process and the subsequent removal of oil-laden OFMSPsC-3 samples using an external magnetic field. In the oil absorption experiments, OFMSPsC-3 demonstrated exceptional efficiency by capturing oil droplets that floated on the water surface within a mere 10 seconds. This rapid absorption is facilitated by the material's superhydrophobic and oleophilic characteristics, combined with its mesoporous structure, which provides ample surface area and pathways for oil uptake. Following absorption, the OFMSPsC-3 was swiftly and effectively attracted to an external magnet, enabling its easy retrieval from the aqueous environment. Importantly, this magnetic separation process left no discernible oil residues in the water, underscoring the material's high selectivity and efficiency in oil–water separation. The high oil-absorption capacity of OFMSPsC-3 is a direct consequence of its synergistic combination of mesoporous architecture and superhydrophobic surface properties. The mesoporous structure ensures a high surface area and interconnected pore networks, which facilitate the rapid uptake and retention of oil molecules. Fig. 5e and f illustrates the oil removal performance of OFMSPsC-3 in practical oil–water separation for both light and heavy oils. As revealed in Fig. 5e and Video S2,† OFMSPsC-3 exhibits excellent adsorption capacity for light oils (e.g., edible oil), rapidly dispersing at the oil–water interface and capturing oil molecules through its superhydrophobic and oleophilic surface properties. Under an applied magnetic field, the OFMSPsC-3 undergoes directional migration from the water surface to the oil layer and ultimately to the magnet, resulting in clear separation with purified water, while the magnetic recovery process requires no additional energy input. Fig. 5f and Video S2† demonstrate the removal of heavy oils (e.g., chloroform). Through surface functionalization, OFMSPsC-3 enhances the oil-particle interfacial affinity, progressively encapsulating and penetrating the heavy oil layer. The mesoporous structure of OFMSPsC-3 provides abundant adsorption
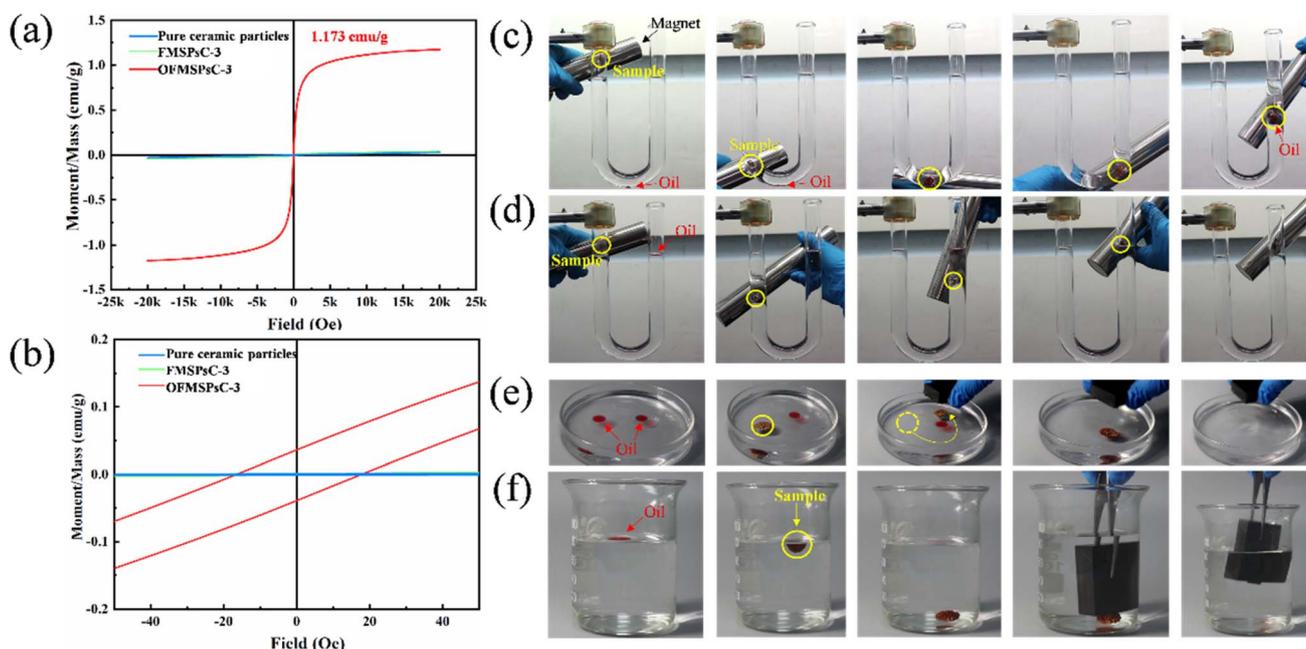

Fig. 5 (a and b) Magnetization hysteresis loops of pure ceramic particles, FMSPs-3 and OFMSPsC-3. (c and d) Magnetic-guided motion and oil cleanup behavior of OFMSPsC-3 within a U-shaped tube. Photograph of OFMSPsC-3 removal of (e) light oil and (f) heavy oil from water.

23054 | J. Mater. Chem. A, 2025, **13**, 23046–23058

This journal is © The Royal Society of Chemistry 2025

sites, ultimately enabling complete oil detachment under the influence of a magnetic field. These results demonstrate that the magnetically guided retrieval capability of OFMSPsC-3, synergized with its mesoporous architecture and superhydrophobicity, enables universal adaptability to diverse oils, offering an efficient strategy for complex oil–water separation.

3.4. The performance and mechanism of oil–water separation

The study evaluated the performance of oil–water separation and the potential separation mechanisms of the superhydrophobic particle filter medium OFMSPsC-3. As displayed in Fig. 6a, the separation procedure employed a gravity-driven filtration system, in which the oil–water mixture was introduced into a funnel filled with OFMSPsC-3 serving as the filtering medium. The material's superhydrophobic and oleophilic properties enabled rapid oil permeation through the filter, while effectively retaining water above it. Fig. 6b demonstrates that, across all tested oil–water systems—including petroleum ether–water, toluene–water, and cyclohexane–water mixtures—the separation efficiency of OFMSPsC-3 exceeded 93%, reaching a maximum of 96.4%. Additionally, for high-viscosity edible oil–water mixtures, the minimum flux of OFMSPsC-3 remained at 0.8 kL m^{-2} h^{-1}, demonstrating its effectiveness in high-viscosity oil–water systems, Table S2†

summarizes and analyzes the separation performance of OFMSPsC across various oil types and concentrations. Throughout the separation process, OFMSPsC-3 effectively managed different oil–water systems, with its remarkable separation efficiency resulting from its superior wettability and hollow mesoporous structural features. To assess the reusability of OFMSPsC-3, ten consecutive oil–water separation cycles were performed. As revealed in Fig. 6c, the separation efficiency remained above 85% across all test cycles, and the flux did not significantly decline, consistently maintaining a level of 4.9 kL m^{-2} h^{-1} (using *n*-hexane–water mixtures as an example). Furthermore, after ten separation cycles, no significant particle detachment was observed on the material's surface, and both the layered roughness and superhydrophobic properties remained stable. This indicates that OFMSPsC-3 possesses excellent durability and reusability, providing strong support for its sustainability in practical oil–water separation applications. The oil adsorption capacity tests demonstrate that OFMSPsC-3 exhibits broad-spectrum effectiveness across oils with varying physicochemical properties (*e.g.*, low-viscosity *n*-hexane/cyclohexane and high-viscosity edible oil). The quantitative results (Fig. S4†) validate its robust oleophilicity and structural porosity, enabling efficient oil uptake. This performance, coupled with the material's magnetic recoverability (Fig. 5c and d), underscores its suitability for practical oil–water
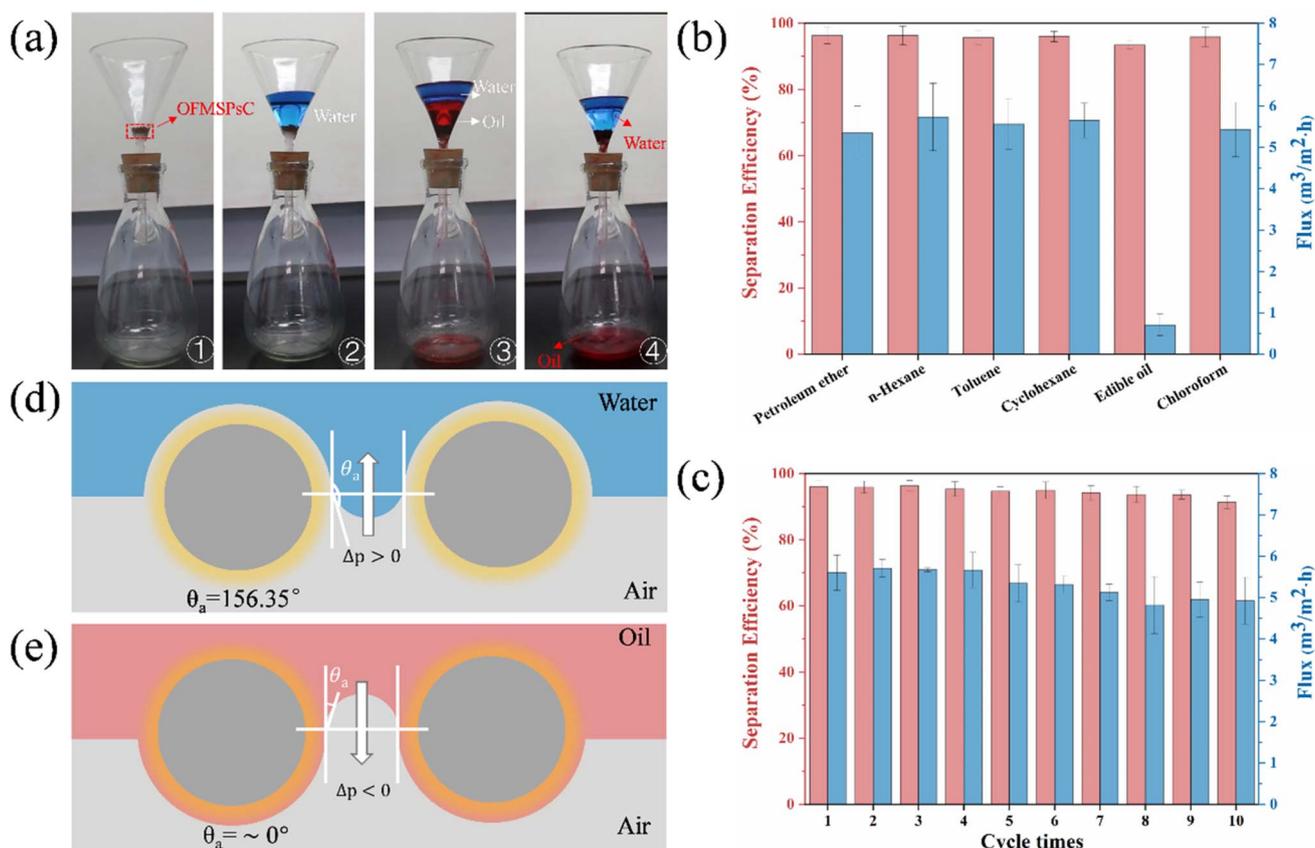

Fig. 6 (a) Equipment and process for oil–water separation. (b) The separation efficiency and flux of the OFMSPsC applied in different kinds of oil/water mixture. (c) The separation efficiency and flux of recirculation separation. (d and e) Mechanism of oil–water separation.

This journal is © The Royal Society of Chemistry 2025

J. Mater. Chem. A, 2025, **13**, 23046–23058 | **23055**

separation scenarios involving diverse oil contaminants. To address the experimental challenges of oil–water separation under varying pH conditions, we investigated the separation efficiency and permeation flux of OFMSPsC material in mixed systems of HCl solution–oil phase, NaCl solution–oil phase, and NaOH solution–oil phase (pH = 1–13). As shown in Fig. S5,† the OFMSPsC material demonstrates exceptional environmental adaptability in oil–water separation applications, maintaining superior performance across a broad pH range (1–13) and in 3.5% NaCl solutions. Experimental results demonstrate stable separation efficiencies of 92.5–95.8%, 92.8–96.0%, and 93.3–96.0% under strongly acidic (pH = 1), neutral (pH = 7), and strongly alkaline (pH = 13) conditions respectively, with typical permeation fluxes reaching 5.49–5.54 kL m^{-2} h^{-1} for chloroform/n-hexane systems. In saline environments, the material achieves over 94% separation efficiency for edible oil–water mixtures and 5.6 kL m^{-2} h^{-1} permeation flux for n-hexane–water systems. This remarkable stability stems from three synergistic factors: the ion-blocking effect of the OTMS hydrophobic layer, the robust chemical stability of the Si–O–Si backbone structure, and optimized surface energy modulation through hierarchical pore engineering. These characteristics collectively validate the material's practical viability in complex operational environments, offering a reliable technical solution for industrial wastewater treatment and marine oil spill remediation applications.

Superhydrophobic OFMSPsC-3 exhibit water contact angles exceeding 150°, preventing water Young–Laplace equation penetration, while oleophilic properties facilitate spontaneous oil passage through the mesoporous framework. This behavior can be explained by the capillary pressure differential predicted by the:[42,43]

$$\Delta p = -2\frac{\gamma_L}{\gamma_p}\cos\theta \qquad (4)$$

where γ_L is the interfacial tension between the liquid and air, γ_p is the pore radius, and θ is the contact angle between the liquid and the solid surface. Fig. 6d and e illustrate that the negative capillary pressure ($\Delta P < 0$) of oil enables its rapid permeation, whereas the positive pressure ($\Delta P > 0$) of water impedes its penetration, ensuring effective separation. Moreover, the robust chemical bonding and molecular entanglement between the OTMS chains, FMSP, and ceramic substrate contribute to the mechanical stability and durability of OFMSPsC-3, enabling it to maintain high separation efficiency through repeated cycles. These comprehensive characteristics render OFMSPsC-3 a highly efficient and sustainable solution for addressing oil–water separation challenges in environmental and industrial applications.

4. Conclusions

In conclusion, the study successfully fabricated a superhydrophobic/oleophilic composite ceramic filter medium (OFMSPsC) by integrating mesoporous silica and magnetic Fe$_3$O$_4$ nanoparticles, followed by modification with OTMS to enhance hydrophobicity and stability. Characterization revealed a contact angle of 156.6° and a saturation magnetization of 1.173 emu g^{-1}. In oil–water separation experiments, OFMSPsC achieved over 93% separation efficiency, with petroleum ether–water systems reaching 96.4% and high-viscosity edible oil–water systems maintaining a minimum flux of 0.8 kL m^{-2} h^{-1}. Ten continuous separation cycles showed efficiencies above 85% and a stable flux of 4.9 kL m^{-2} h^{-1}. The embedded magnetic nanoparticles enabled rapid oil recovery within 10 seconds using an external magnetic field, significantly enhancing reusability and operational convenience. Acid–base tests confirmed contact angles above 140° across a pH range of 1 to 13, and thermal stability assessments showed excellent superhydrophobicity below 200 °C. Overall, OFMSPsC exhibits exceptional performance for oil–water separation, promising applications in environmental remediation and industrial oil spill cleanup.

Data availability

All data supporting the findings of this study are available within the article and its additional files.

Conflicts of interest

The authors confirm that they have no conflicts of interest.

Acknowledgements

References

1 S. Ning, G. Tian and F. Yang, Bionic silanized cellulose superhydrophobic paper for efficient oil–water separation, *Sep. Purif. Technol.*, 2025, **353**, 128523, DOI: **10.1016/j.seppur.2024.128523**.

2 B. Wang, W. Liang, Z. Guo and W. Liu, Biomimetic super-lyophobic and super-lyophilic materials applied for oil/water separation: A new strategy beyond nature, *Chem. Soc. Rev.*, 2015, **44**, 336–361, DOI: **10.1039/c4cs00220b**.

3 J. Zhou, W. Lin, Y. Yu, C. Dong, H. Zhang, Z. Hu and C. Kao, Transitioning weathered oil fields towards new energy: A review on utilizing hydrogenotrophic methanogens for petroleum hydrocarbons remediation, *J. Hazard. Mater.*, 2024, 135279, DOI: **10.1016/j.jhazmat.2024.135279**.

4 M. Wang, Migration rules of petroleum pollutants in water and soil: a review, *Pet. Sci. Technol.*, 2024, **42**, 4281–4296, DOI: **10.1080/10916466.2023.2223596**.

23056 | *J. Mater. Chem. A*, 2025, **13**, 23046–23058

This journal is © The Royal Society of Chemistry 2025

5   B. Liu, B. Chen, J. Ling, E. J. Matchinski, G. Dong, X. Ye, F. Wu, W. Shen, L. Liu, K. Lee, L. Isaacman, S. Potter, B. Hynes and B. Zhang, Development of advanced oil/water separation technologies to enhance the effectiveness of mechanical oil recovery operations at sea: Potential and challenges, *J. Hazard. Mater.*, 2022, **437**, 129340, DOI: **10.1016/j.jhazmat.2022.129340**.

6   B. Xiang, J. Gong, Y. Sun, W. Yan, R. Jin and J. Li, High permeability PEG/MXene@ MOF membrane with stable interlayer spacing and efficient fouling resistance for continuous oily wastewater purification, *J. Membr. Sci.*, 2024, **691**, 122247, DOI: **10.1016/j.memsci.2023.122247**.

7   G. Yang, Y. Zhang, Z. Yin, Y. Deng, Z. Li, Y. Xie, Y. Chen, C. Yang, H. Yang, Y. Luo, Z. Hong and M. Xue, Robust mussel-inspired LBL carbon nanotube-based superhydrophobic polyurethane sponge for efficient oil–water separation utilizing photothermal effect, *Fuel*, 2025, **381**, 133353, DOI: **10.1016/j.fuel.2024.133353**.

8   J. Gong, B. ang, Y. Sun and J. Li, Janus smart materials with asymmetrical wettability for on-demand oil/water separation: a comprehensive review, *J. Mater. Chem. A*, 2023, **46**, 25093–25114, DOI: **10.1039/D3TA04160C**.

9   Y. Deng, C. Peng, M. Dai, D. Lin, I. Ali, S. S. Alhewairini, X. Zheng, G. Chen, J. Li and I. Naz, Recent development of super-wettable materials and their applications in oil-water separation, *J. Cleaner Prod.*, 2020, **266**, 121624, DOI: **10.1016/j.jclepro.2020.121624**.

10 Q.-Y. Cheng, X.-P. An, Y.-D. Li, C.-L. Huang and J.-B. Zeng, Sustainable and biodegradable superhydrophobic coating from epoxidized soybean oil and ZnO nanoparticles on cellulosic substrates for efficient oil/water separation, *ACS Sustainable Chem. Eng.*, 2017, **5**, 11440–11450, DOI: **10.1021/acssuschemeng.7b02549**.

11 Y. Zhu, T. Zhang, H. Liu, C. Jin, C. Feng, J. Huang, H. Na and J. Zhu, Superhydrophobic microporous membrane based on modified microfibrillated cellulose framework for efficient oil-water separation, *Int. J. Biol. Macromol.*, 2024, **279**, 135163, DOI: **10.1016/j.ijbiomac.2024.135163**.

12 M. Zhang, H. Ning, J. Shang, F. Liu and S. Peng, A robust superhydrophobic-superoleophilic PDMS/Al$_2$O$_3$/CM composite ceramic membrane: Stability, efficient emulsified oil/water separation, and anti-pollution performance, *Sep. Purif. Technol.*, 2024, **328**, 124864, DOI: **10.1016/j.seppur.2023.124864**.

13 W. Yang, B. Yao, L. Chai, G. Yang and L. Deng, Multifunctional conductive sponge with excellent superhydrophobicity, piezoresistivity, electro/light to heat conversion, and oil/water separation performance, *Chem. Eng. J.*, 2022, 140532, DOI: **10.1016/j.cej.2022.140532**.

14 J. Yuan, X. Liu, O. Akbulut, J. Hu, S. L. Suib, J. Kong and F. Stellacci, Superwetting nanowire membranes for selective absorption, *Nat. Nanotechnol.*, 2008, **3**, 332–336, DOI: **10.1038/nnano.2008.136**.

15 X. Zhang, C. Hu, J. Lin, H. Yin, J. Shi, J. Tang, B. Ma, T. Li and K. Ren, Fabrication of recyclable, superhydrophobic-superoleophilic quartz sand by facile two-step modification for oil-water separation, *J. Environ. Chem. Eng.*, 2022, **10**, 107019, DOI: **10.1016/j.jece.2021.107019**.

16 F. Xiao, H. Zhang, T. Wu, J. Liu, J. Liu, J. Zhang, W. Liu, T. Liang and J. Hu, Superhydrophobic/superlipophilic interface layer for oil-water separation, *Process Saf. Environ. Prot.*, 2022, **161**, 13–21, DOI: **10.1016/j.psep.2022.01.043**.

17 L. Lin, S. Wu, Z. Ai, M. Pan, C. Wu, W. Zhang, Z. Li and Z. Zhou, Superhydrophobic Composite Sponge with Magnetically Driven and Photo-Thermal Conversion Performance for Efficient Oil-Water Separation, *Process Saf. Environ. Prot.*, 2025, 106801, DOI: **10.1016/j.psep.2025.106801**.

18 M. Yu, C. Ma, C. Liao, Y. Wang and D. Wang, Preparation and oil-water separation performance of lignin-based durable superhydrophobic petaloid structure inspired from springtail cuticle surface, *Prog. Org. Coat.*, 2025, **198**, 108907, DOI: **10.1016/j.porgcoat.2024.108907**.

19 X. Li, L. Han, Z. Huang, Z. Li, F. Li, H. Duan, L. Huang, Q. Jia, H. Zhang and S. Zhang, A robust air superhydrophilic/superoleophobic diatomite porous ceramic for high-performance continuous separation of oil-in-water emulsion, *Chemosphere*, 2022, **303**, 134756, DOI: **10.1016/j.chemosphere.2022.134756**.

20 L. Han, X. Li, F. Li, H. Zhang, G. Li, Q. Jia and S. Zhang, Superhydrophilic/air-superoleophobic diatomite porous ceramics for highly-efficient separation of oil-in-water emulsion, *J. Environ. Chem. Eng.*, 2022, **10**, 108483, DOI: **10.1016/j.jece.2022.108483**.

21 Z. Liu, Y. Si, C. Yu, L. Jiang and Z. Dong, Bioinspired superwetting oil–water separation strategy: toward the era of openness, *Chem. Soc. Rev.*, 2024, **53**, 10012–10043, DOI: **10.1039/d4cs00673a**.

22 S. He, Y. Zhan, Y. Bai, J. Hu, Y. Li, G. Zhang and S. Zhao, Gravity-driven and high flux super-hydrophobic/super-oleophilic poly(arylene ether nitrile) nanofibrous composite membranes for efficient water-in-oil emulsions separation in harsh environments, *Composites, Part B*, 2019, **177**, 107439, DOI: **10.1016/j.compositesb.2019.107439**.

23 H. Wang, M. Wang, Y. Wang, J. Wang, X. Men, Z. Zhang and V. Singh, Synergistic effects of COF and GO on high flux oil/water separation performance of superhydrophobic composites, *Sep. Purif. Technol.*, 2021, **276**, 119268, DOI: **10.1016/j.seppur.2021.119268**.

24 A. B. M. Giasuddin, A. Cartwright, K. Jackson and D. W. Britt, One-Step Hydrophobic Silica Nanoparticle Synthesis at the Air/Water Interface, *ACS Sustain. Chem. Eng.*, 2019, **7**, 6204–6212, DOI: **10.1021/acssuschemeng.8b06359**.

25 F. Wang, R. Ma, J. Zhan, T. Wang and Y. Tian, Superhydrophobic starch-based cryogels modified with silylated magnetic nanoparticles for oil spill cleanup, *J. Cleaner Prod.*, 2022, **363**, 132492, DOI: **10.1016/j.jclepro.2022.132492**.

26 Q. Li and Z. Guo, Lubricant-infused slippery surfaces: Facile fabrication, unique liquid repellence and antireflective properties, *J. Colloid Interface Sci.*, 2019, **536**, 507–515, DOI: **10.1016/j.jcis.2018.10.083**.

This journal is © The Royal Society of Chemistry 2025

J. Mater. Chem. A, 2025, **13**, 23046–23058 | **23057**

27 T. H. Kim and K. C. Song, Low-temperature preparation of superhydrophilic coatings using tetraethoxysilane and colloidal silica by sol-gel method, *Colloids Surf., A*, 2022, **647**, 129105, DOI: **10.1016/j.colsurfa.2022.129105**.

28 L. G. Arellano-Galindo, A. C. Reynosa-Martínez, J. R. Gaitán-Arévalo, M. F. Valerio-Rodríguez, G. Vargas-Gutiérrez and E. López-Honorato, Superhydrophobic to superhydrophilic wettability transition of functionalized SiO$_2$ nanoparticles, *Ceram. Int.*, 2022, **48**, 21672–21678, DOI: **10.1016/j.ceramint.2022.04.137**.

29 J. Ma, Y. Qing, H. Song, Y. Yao, X. Xu, C. Long, M. Cui, M. Han and C. Liu, High-Performance, Superhydrophobic, and Wearable Strain Sensor for Amphibious Human Motion Detection, *Adv. Mater. Technol.*, 2022, 2200798, DOI: **10.1002/admt.202200798**.

30 K. Hu, H. Lyu, H. Duan, Z. Hu and B. Shen, Facilitate the preparation of naturally modified and self-healing superhydrophobic/superoleophilic biochar-based foams for efficient oil-water separation, *J. Hazard. Mater.*, 2024, **465**, 133489, DOI: **10.1016/j.jhazmat.2024.133489**.

31 N. Rabiee, M. Atarod, M. Tavakolizadeh, S. Asgari, M. Rezaei, O. Akhavan, A. Pourjavadi, M. Jouyandeh, E. C. Lima, A. Hamed, A. Ehsani, S. Ahmadi and M. Reza, Materials Green metal-organic frameworks (MOFs) for biomedical applications, *Microporous Mesoporous Mater.*, 2022, **335**, 111670, DOI: **10.1016/j.micromeso.2021.111670**.

32 M. khalilifard and S. Javadian, Magnetic superhydrophobic polyurethane sponge loaded with Fe$_3$O$_4$@oleic acid@graphene oxide as high performance adsorbent oil from water, *Chem. Eng. J.*, 2021, **408**, 127369, DOI: **10.1016/j.cej.2020.127369**.

33 R. Fang, R. Liu, Z. H. Xie, L. Wu, Y. Ouyang and M. Li, Corrosion-resistant and superhydrophobic nickel phosphorus/nickel/PFDTMS triple-layer coating on magnesium alloy, *Surf. Coat. Technol.*, 2022, **432**, 128054, DOI: **10.1016/j.surfcoat.2021.128054**.

34 F. Wang, R. Ma and Y. Tian, Superhydrophobic starch-based nanocomposite cryogel for oil removal underwater and magnetically guided oil slick cleanup, *Carbohydr. Polym.*, 2022, **287**, 119297, DOI: **10.1016/j.carbpol.2022.119297**.

35 F. Wang, R. Ma and Y. Tian, Fabrication of superhydrophobic/oleophilic starch cryogel *via* a simple sol-gel immersion process for removing oil from water,

Ind. Crops Prod., 2022, **184**, 115010, DOI: **10.1016/j.indcrop.2022.115010**.

36 Z. Chen, X. Su, K. Li, S. Niu, Z. Shen, X. Li, S. Chen and W. Wu, A thiolated TiO$_2$-based degradable superhydrophobic wood for oil–water separation and heavy metal treatment, *Sep. Purif. Technol.*, 2025, **354**, 128949, DOI: **10.1016/j.seppur.2024.128949**.

37 H. Sun, Z. Liu, K. Liu, M. E. Gibril, F. Kong and S. Wang, Lignin-based superhydrophobic melamine resin sponges and their application in oil/water separation, *Ind. Crops Prod.*, 2021, **170**, 113798, DOI: **10.1016/j.indcrop.2021.113798**.

38 X. Wang, H. Zhang and Y. Qing, Long-lived superhydrophobic micro/nano-locked fiber membranes for long-lasting oil-water separation effectiveness, *Sep. Purif. Technol.*, 2025, **358**, 130237, DOI: **10.1016/j.seppur.2024.130237**.

39 C. H. Hoang, T. T. Nguyen, D. Q. Ho, H. V. Le and H. H. Nguyen, Fabrication of superhydrophobic surfaces for applications in total internal reflection effects, *Mater. Today Commun.*, 2023, **35**, 105928, DOI: **10.1016/j.mtcomm.2023.105928**.

40 T. Wei, X. Fan, Q. Cheng, J. Cai, Y. Wang, J. Wang, Z. Xu, Y. Shuai, Q. Wan, Y. Chen and M. Yang, Design of fluorine-free superhydrophobic silk fabrics with mechanical durability and self-cleaning properties for oil-water separation, *Surf. Interfaces*, 2024, **48**, 104279, DOI: **10.1016/j.surfin.2024.104279**.

41 Z. Shi, H. Zeng, Y. Yuan, N. Shi, L. Wen, H. Rong, D. Zhu, L. Hu, L. Ji, L. Zhao and X. Zhang, Constructing Superhydrophobicity by Self-Assembly of SiO$_2$@Polydopamine Core-Shell Nanospheres with Robust Oil-Water Separation Efficiency and Anti-Corrosion Performance, *Adv. Funct. Mater.*, 2023, **33(16)**, 2213042, DOI: **10.1002/adfm.202213042**.

42 C. Long, X. Long, Y. Cai, X. Wang, C. Li, Y. Qing and Y. Zhao, Long-lived nanoparticle-embedded superhydrophobic membranes with rapid photocatalytic properties and continuous oil-water separation, *Chem. Eng. J.*, 2024, 148743, DOI: **10.1016/j.cej.2024.148743**.

43 R. Jin, J. Gong, B. Xiang and J. Li, Biomass materials with special wettability: a sustainable solution for efficient oil-water separation, *J. Mater. Chem. A*, 2024, 23315–23336, DOI: **10.1039/d4ta04039b**.

23058 | *J. Mater. Chem. A*, 2025, **13**, 23046–23058

This journal is © The Royal Society of Chemistry 2025